

M. Thieme · H. Worch

## Ultrahydrophobic aluminium surfaces: properties and EIS measurements of different oxidic and thin-film coated states

Received: 29 May 2005 / Accepted: 9 November 2005 / Published online: 3 May 2006  
© Springer-Verlag 2006

**Abstract** Firstly, the contribution summarises important results of the work dedicated to the formation of ultrahydrophobic aluminium surfaces. This treatment comprises sulphuric acid anodisation under intensified temperature and current density conditions ('SAAi') as well as subsequent chemical modification ('C'). The usual sulphuric acid anodisation ('SAAu') was included for comparison. These various states were examined by electrochemical impedance spectrometry (EIS) to derive typical EIS-related features, especially for the ultrahydrophobic states compared to the anodised surfaces. Based on well-defined spectra types, modelling yielded results, preferentially with regard to the nano-porosity of the oxidic layers. EIS measurements allowed the conclusion that the original nano-porosity underwent specific changes due to the chemical modification variants employed. The chances of EIS predicting the stability of the ultrahydrophobically modified systems are critically assessed on the background of standardised weathering tests.

**Keywords** Aluminium · Anodisation · Oxide layer · Ultrahydrophobicity · Electrochemical impedance spectrometry

### Introduction

The anodic oxidation of aluminium materials has clearly gained enormous importance since the 1920s, both from a scientific point of view and for technology and industrial production [1, 2]. Correspondingly, Kurt Schwabe, who devoted much of his scientific productivity to corrosion and passivity, took up issues concerning not only iron metals, but also the specific behaviour of aluminium and

other valve metals (compiled in [3]). Utilising radioactive labelling ( $T_2O$ ,  $H_2^{35}SO_4$ ), one of his numerous works focussed on the dehydration effects and uptake of anion-derived species into the gel-like oxidic layer during the anodic oxidation process of Al [4]. The importance of the anodic oxidation of Al has continued into present developments of acid-generated anodic layers with self-ordered nanoporous structures as a template for data storage [5].

Additionally, the anodisation has opened up another promising application field: It is possible to generate micro-rough surfaces and, by means of subsequent fixation of hydrophobic organic compounds, ultrahydrophobicity [7–9]. Within the research work that is referred to in this contribution, the sulphuric acid anodisation process (usually abbreviated 'SAA') was modified in its temperature, current density and duration parameters so that the growth of the oxidic layer was accompanied by etch-like dissolution effects and the formation of a micro-rough surface [8, 9]. Similar parameter variations had been carried out earlier, unbeknownst to the present authors [6]; however, Strawbridge and co-workers used considerably higher current densities, focussing particularly with regard to mechanical properties of the produced oxidic layers. It should be mentioned that basic botanical studies have provided important impulses in the sense of bionics [10–12]. At present, theoretical aspects of ultrahydrophobicity are still intensively studied [13–15]. Furthermore, based on first practical use of ultrahydrophobic parts, additional useful fields of application are being envisaged, e.g. Al-based self-cleaning facades [8, 9, 16]. Hopefully, the generation of such a property profile will not only facilitate the removal of dirt, but also make a contribution for optimising corrosion protection measures by means of the exclusion of water. It is interesting that the role of water as a prerequisite and promoter for passivation was also studied by Schwabe [17].

Electrochemical impedance spectrometry (EIS) has established an effective testing method preferably for anodised Al or organically coated materials [18–23]. The effect of the roughness of solid electrodes on the impedance properties represents a special issue which has been

M. Thieme (✉) · H. Worch  
Technische Universität Dresden,  
Institut für Werkstoffwissenschaft,  
01062 Dresden, Germany  
e-mail: michael.thieme@tu-dresden.de  
Tel.: +49-351-46336461  
Fax: +49-351-46333207

vastly studied by several research groups [25–28]. Roughness was related with constant-phase elements in the equivalent circuit (Eqc) instead of a pure capacitance, both for blocked electrodes and electrodes with a Faradaic current with and without diffusion control. The strictly geometrically based consideration was recently amended by different cases where dielectric surface layers occurred with distributed conductivity and/or permittivity properties perpendicularly to the surface [27]. However, combined rough and porous electrodes were actually not treated with regard to their EIS behaviour.

The use of silanes, phosphonic acids and other agent groups for the formulation of coatings for corrosion protection is the object of intensive investigation [29–32]. Van Ooij and co-workers indicated the wide applicability of silanes and bis-silanes as anticorrosion agents, also tracing interface and degradation processes by means of EIS [29]. With regard to the use of adhesion promoters at the metal-coating interface, it was stated for smooth sputtered aluminium [32] that the specific head group functionalities and the chain lengths of the molecules influenced the packaging density of the self-assembling monolayers (SAM) formed. Alkyl phosphonic and carboxylic acids gave the most well-packed SAMs in comparison with silanes. However, the authors also observed diminished water stability of phosphonic acid adsorbates.

The first part of this contribution summarises results of the work dedicated to the formation of ultrahydrophobic aluminium surfaces. The major treatment pathway consists of the following sequence: pickling (abbr. ‘P’)/anodisation in sulphuric acid medium under intensified temperature and current density conditions (‘SAAi’)/chemical modification by hydrophobic films coating (‘C’) using solutions of an alkanephosphonic acid, a fluorine-substituted alkyl silane and the fluoro-copolymer Teflon® AF, respectively [9]. The usual sulphuric acid anodisation (‘SAAu’) was accomplished for comparison. It should be noted that the modification step leads to very thin films (or even SAMs) which do not affect the primary morphology. Thus, this surface type is completely different from coating systems where much thicker organic layers are applied as a measure of corrosion protection. Additionally, sealing measures were investigated [23], but this is not the subject of the present contribution.

With this background, Part 2 presents EIS properties of the specific surface types generated by the treatment mentioned above (P; P/SAAi; P/SAAu; P/SAAi/C; P/SAAu/C). Test solutions of moderately acid character (pH=6 and 4, respectively) were employed to avoid or to limit corrosion reactions of the oxide-covered metal. The results of EIS-based modelling are preferentially analysed in terms of inherent nano-porosity properties. The changes measured over exposure in electrolyte solutions are compared with the results of a representative standardised test (DIN EN ISO 11341) relating to the evaluation of the stability of different coating systems under water and light exposure.

## Experimental

### Materials

Pure aluminium EN AW-Al 99.5 (EN AW-1050) and the alloy Al Mg1 (EN AW-5005) were used as sheet specimens ( $26 \times 38 \times 1 \text{ mm}^3$ ) for process development and characterisation. For EIS, rod-shaped specimens ( $\varnothing 5 \text{ mm}$ ) of Al MgSi0.5 (EN AW-5060) were employed.

### Pickling (‘P’)

All the specimens initially underwent a cleaning pre-treatment, consisting of alkaline pickling (1 M NaOH, ambient temperature, 0.6 ks), neutralising (1 M HNO<sub>3</sub>, 60 s) and water rinsing.

### Anodisation

For micro-roughening, the specimens were treated under SAAi conditions: stirred H<sub>2</sub>SO<sub>4</sub>–Al<sub>2</sub>(SO<sub>4</sub>)<sub>3</sub> solutions with the concentrations  $c$  (total sulphate)=2.3 mol l<sup>-1</sup> and  $c(\text{Al}^{3+})_{\text{max}}=0.36 \text{ mol l}^{-1}$ , temperature  $T=(40 \pm 1)^\circ\text{C}$ , current density  $j=28\text{--}30 \text{ mA cm}^{-2}$ , duration  $t=1.2 \text{ ks}$ . The specimens were rinsed and water-immersed for at least 3.6 ks. The SAAu procedure was applied under the conditions 18–20 °C, 15 mA cm<sup>-2</sup>, 1.5 ks. Mass changes were measured by weighing, where  $m_1$ —starting mass,  $m_2$ —mass after anodisation,  $m_3$ —mass after stripping the layer in a small volume of 1 M H<sub>2</sub>SO<sub>4</sub> and 0.7 M HCl, respectively (40 °C, 2.4 ks). These values were corrected for the (low) substrate material attack. The morphology was examined by scanning electron microscopy (Zeiss DSM 982 Gemini) using an accelerating voltage of 2 kV. The mass of dissolved Al(III) contained in the oxide stripping solution,  $m_{\text{Al,ox}}$ , was determined by complexometric titration [33].

### Chemical modification (‘C’)

The following substances were employed:

1. tetradecanephosphonic acid (TDPA) (0.1 wt% in ethanol–water 1+1, 12 h),
2. perfluoroalkyltriethoxysilane (PFATES) (2 vol% in *t*-butylmethylether, 3 h),
3. 3-(2-Aminoethylamino)propyltrimethoxysilane (AEAPS) (10 vol% in ethanol, 3 h) followed by the fluoropolymer poly(tetrafluoroethylene-*co*-2,2'-bis(trifluoromethyl)-4,5-difluoro-1,3-dioxole) (Teflon® AF; DuPont) (0.6 wt% in perfluoro-(2-perfluoro-*n*-butyl)-tetrahydrofuran (FC75; 3 M)).

The modification was completed by tempering at 120 °C, 1 h. The wetting properties were characterised by dynamic contact angle measurements (Krüss DSA10; advancing angle  $\theta_a$ , receding angle  $\theta_r$ ) based on 3–5 sites on each specimen.

## Electrochemical impedance spectrometry

The specimens represented the stages P, P/SAAi, P/SAAu, P/SAAi/C and P/SAAu/C. Two test electrolyte types were employed: 1)  $\text{Na}_2\text{SO}_4$  0.5 mol l<sup>-1</sup>, pH=4.0, 2) phosphate buffer (PB) with  $c(\text{total phosphate})=0.133 \text{ mol l}^{-1}$ , pH=6.0, each under air contact and at ambient temperature. The immersion depth of the rods during EIS was 10 mm less than that during the previous preparative steps (effective EIS areas 8.05 and 4.1 cm<sup>2</sup>, respectively). A conventional three-electrode measuring cell (KMZ 3, Sensortechnik Meinsberg, Germany) with a symmetrically positioned Pt net as counter electrode was combined with the instruments VoltaLab 40/PGZ 301 (Radiometer Analytical, France) or IM 6 (Zahner, Germany). The measurements were performed at open circuit potential (ocp) in the frequency range  $10^5$ – $10^{-3}$  Hz. Auto-ranging difficulties encountered with the VoltaLab system in the HF range were overcome using a series resistor of appropriate height, whose EIS response was subtracted afterwards. In addition to the first measurement soon after immersion (EIS start after 0.5 h, ‘instantaneous’), further EIS measurements were started, at maximum after 18 h immersion. At least two specimens of each type were examined. Modelling was done by means of the ZView software (Scribner, USA), which contains the LEVM 6.0 programme by RossMacdonald. Constant phase elements of the form  $Z(CPE) = 1/[C(i\omega)^\alpha]$  were used in addition to resistances and capacitances. Elements referring to diffusion control were abandoned. The goodness of fit was judged from the chi-squared test ( $\chi^2$ ) using the original data before area correction.

## Stability characterisation

Amongst other tests, the simulating weathering test according to DIN EN ISO 11341, Zyklus A, was applied. It comprises alternating moistening and drying (period length 2 h) combined with Xenon lamp radiation (exposure 360 h; Institut für Korrosionsschutz Dresden GmbH). P/SAAi/C-specimens with TDPA, PFATES or Teflon® AF modification (four of each) were tested.

## Results and discussion

### Characteristics of the intensified anodisation process

As Fig. 1 shows, the chronopotentiometric curve for the anodic process under intensified conditions (SAAi) is characterised by an initially steep potential rise, which is ascribed to the buildup of the barrier oxide film adjacent to the metal substrate. Thereafter, a potential plateau is formed at a somewhat lower level. The potential heights reflect also the different conductivity of the solutions according to the varying H<sup>+</sup>-to-Al<sup>3+</sup> ratio. Under usual anodisation conditions (SAAu), a similar curve is recorded, however, on higher potentials.

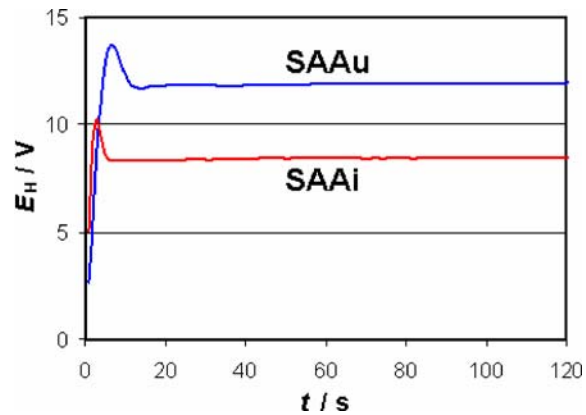


**Fig. 1** Starting sections of potential-time curves for the anodisation under intensified (SAAi) and usual (SAAu) conditions, respectively;  $c(\text{SO}_4^{2-})=2.3 \text{ mol l}^{-1}$ ,  $c(\text{Al}^{3+})=0.04 \text{ mol l}^{-1}$

Further insight into the intensified anodisation process was gained from the analysis of the mass parameters  $\Delta m/A$  for varied anodisation times up to a maximum of 1.8 ks, which include the regular duration. Figure 2 gives the courses in dependence on the charge density  $q$ . The values of  $(m_2-m_1)/A$  pass a shallow maximum for anodisation times of about 0.3 ks and move into the negative range beyond 0.6 ks. This means the specimens undergo increasing mass loss. The specific oxide mass  $(m_2-m_3)/A$  increases up to a limiting value of about 2.5 mg cm<sup>-2</sup> for anodisation times of more than 1.2 ks, disregarding the potential constancy from about 10 s on. The overall metal mass loss  $(m_3-m_1)/A$  changes linearly with the charge passed, thereby coinciding with a curve based on Faraday’s law. This means that the transformation of Al into Al(III) proceeds exclusively on an electrochemical basis. Thus, the quantity  $(m_3-m_1)/A$  may be substituted by the charge density  $q$ .

The degree of oxidic layer formation within the total anodic process was characterised by the oxide formation efficiency  $\varepsilon_{\text{ox}}$ . This quantity is defined as the ratio of the oxidised Al(III) bound in the layer  $m_{\text{Al},\text{ox}}$  and the total metal mass loss  $(m_3-m_1)$ . Clearly, this is a better approach

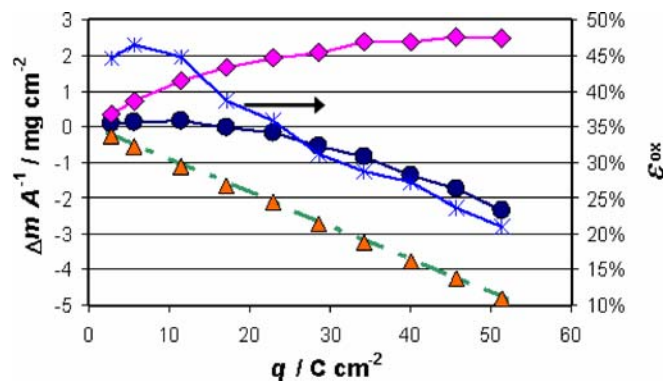
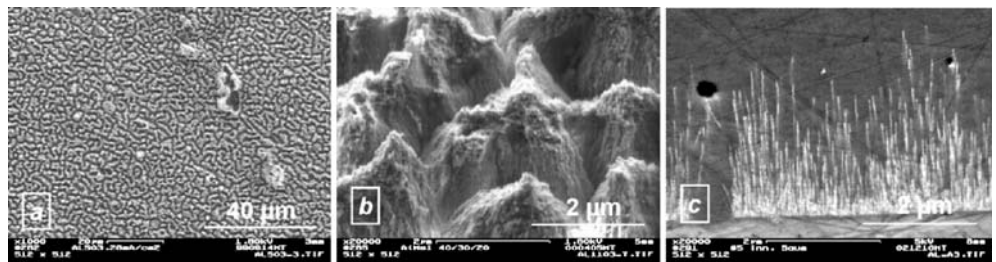


**Fig. 2** Characteristics of the SAAi process (medium stirring intensity) for experiments with varied anodic charge density  $q$ : specific mass changes  $(m_2-m_1)/A$  (-●-),  $(m_2-m_3)/A$  (-◆-),  $(m_3-m_1)/A$  (-▲-), specific metal mass loss according to Faraday’s law (- - -) and oxide formation efficiency  $\varepsilon_{\text{ox}}$  (\*); means of 2–8 single data

**Fig. 3** SEM images of Al Mg1 after P/SAAi treatment; **b** specimen 35° tilted; **c** visualisation of the nano-porosity by cathodic deposition of Sn/Cu into the pore grounds of the porous sub-layer, followed by cross-sectioning



than in [6], where the efficiency was calculated using inappropriate data for the composition of the oxidic layer and its density. The oxide formation efficiency was found here to be about 45 wt% maximum at the starting phase of the anodisation, whereupon it decreases with increasing duration in a practically linear manner (Fig. 2). It should be noted that the relatively low efficiency values of 25–30% under the regular SAAi conditions is disadvantageous from an economic point of view. However, this is a consequence of the superimposing reactions of oxide formation and dissolution which lead to the specific morphology (see below) as the major target of the anodic treatment. Similar results were obtained with Al 99.9 and Al Mg1.

The oxide formation efficiency for the SAAu process is much higher due to the lower temperature. Comparative measurements gave values of nearly 80 wt%.

#### Features of the anodised surfaces

The SAAi process gives the surface a specific *morphology* characterised by irregularly ordered mountain-like structure elements of typically 1–2  $\mu\text{m}$  in distance and height (Fig. 3a,b), which is similar to the findings in [6]. Additionally, a very fine, fibre-like roughness can be seen in the sub- $\mu\text{m}$ -scale (Fig. 3b). In contrast, the SAAu-treated surfaces are characterised by a more or less flat,

shell-like shaped morphology of the oxidic layer, as documented earlier [8, 9].

The micro-roughness features of SAAi surfaces have been proved to be one of the key factors for generating ultrahydrophobicity. It was achieved during numerous experiments to define ‘process windows’ (temperature, current density, stirring, duration) for a successful anodic treatment [9]. Interestingly, the low-temperature, low-current-density anodisation conditions, as described by Tsujii et al. [7], failed in generating an appropriate type of micro-roughness as prerequisite for ultrahydrophobicity.

Information on *structural and composition features*, which had been gained earlier [9], is briefly summarised here. Microscopic and SEM examinations of cross-sectioned SAAi specimens showed that the thickness data are quite similar compared to those following the SAAu treatment (10–12  $\mu\text{m}$ ). From stripping experiments and the thickness, a density of about  $2.3 \text{ g cm}^{-3}$  is estimated for the SAAi layer. SEM points to a similar structure of the nanoporous sub-layers with a somewhat higher lateral pitch for SAAi (Fig. 3c). As etching experiments indicated, the chemical stability of the porous sub-layer is non-uniform over its depth. This applies also for its hardness, as the most recent nano-hardness measurements (max. 16 mN) showed. The substance is amorphous according to X-ray diffraction, with  $\text{AlO}_4$ ,  $\text{AlO}_5$  and  $\text{AlO}_6$  coordination, as detected by  $^{27}\text{Al}$  nuclear magnetic resonance. The portion

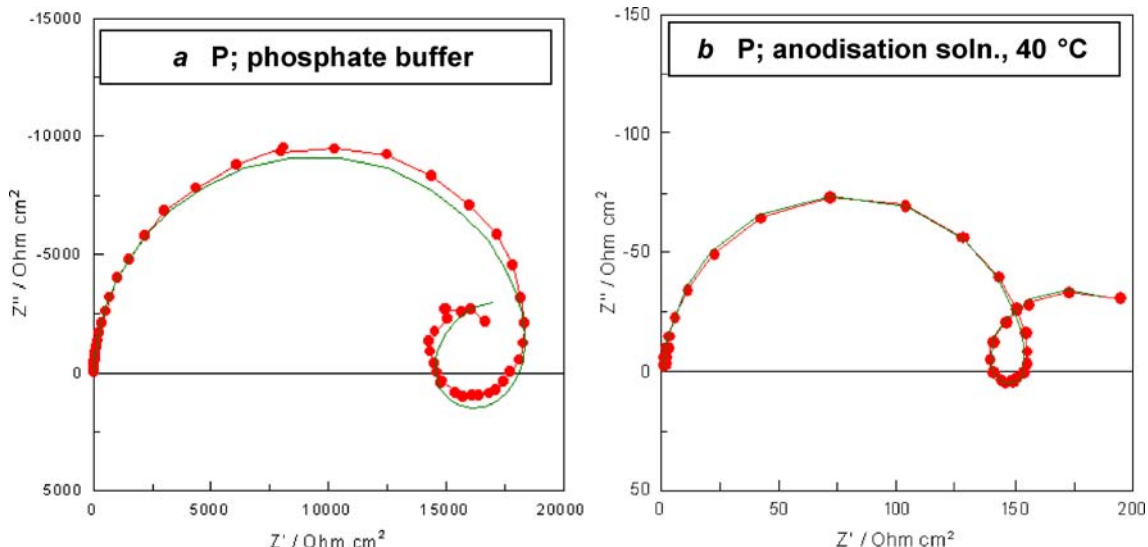


**Fig. 4** Nyquist plots for pickled surfaces under different test conditions (-●-) together with the fitted curves (—) based on the equivalent circuit Eqc I

**Table 1** Numerical values based on model Eqc I for pickled surfaces in different test solutions

|                                 | $R_1/\Omega \text{ cm}^2$ | $R_2/\text{k}\Omega \text{ cm}^2$ | $\text{CPE}_2/\mu\text{F cm}^{-2}$ | $R_3/\text{k}\Omega \text{ cm}^2$ | $C_3/\text{mF cm}^{-2}$ | $R_4/\text{k}\Omega \text{ cm}^2$ | $C_4/\text{mF cm}^{-2}$ | $\chi^2$ |
|---------------------------------|---------------------------|-----------------------------------|------------------------------------|-----------------------------------|-------------------------|-----------------------------------|-------------------------|----------|
| Na <sub>2</sub> SO <sub>4</sub> | 6.93                      | 84.3                              | 5.99 (0.910)                       | -31.8                             | -0.179                  | 339                               | 1.59                    | 0.0066   |
| Phosphate buffer                | 5.28                      | 18.9                              | 9.98 (0.981)                       | -4.58                             | -0.821                  | 6.26                              | 29.2                    | 0.0182   |
| Anodisation soln., 40°C         | 1.38                      | 0.154                             | 13.0 (0.977)                       | -0.0180                           | -14.5                   | 0.0709                            | 5.69                    | 0.00207  |

Contact areas are accounted for; CPE: parameters  $C$  and  $\alpha$  (in brackets) given

of Al(III) in the layer substance amounts to 34–41 wt% with an increasing tendency in the course of anodisation. In addition to a considerable portion of water (markedly more than in SAAu layers according to gravimetric, infrared and nuclear analytical examinations), the layer also contains sulphate (ca. 17 wt%). From all these data, the following approximate formula was derived:  $\text{Al}_2[\text{O}_{3-y-z/2} (\text{SO}_4^{2-})_y (\text{HSO}_4^-)_z] x\text{H}_2\text{O}$  with  $x \approx 0.52$ ,  $z \approx 0.24$  and  $y \ll z$ .

### Chemical modification and wetting properties

Extensive selection tests had been carried out for choosing suitable hydrophobic compounds which differently react to the hydroxylated surface [8, 9, 16]. Thus, the initially hydrophilic micro-rough SAAi surface can be successfully treated using quite different compound groups, such as long-chain carbonic acids, differently functionalised reactive alkyltrialkoxysilanes, alkylchlorosilanes, alkanephosphonic acids, fluoropolymers or polyelectrolyte/surfactant complexes. According to dynamic contact angle measurements, the angles were in the range of 150–160° with mostly negligible hysteresis  $\theta_a - \theta_r$ .

### EIS results and modelling

#### Pickled surfaces ( $P$ )

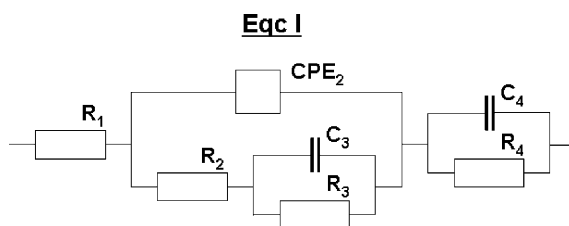
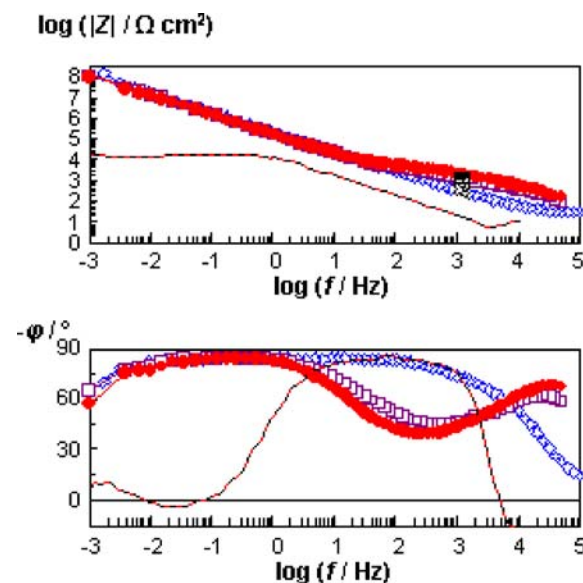
This surface type represents the starting point for the following treatments. The spectra, recorded with generally freshly prepared surfaces and practically inert solutions, showed a prominent semicircle in the Nyquist plot, which was provided with a low-frequency loop appendix (Fig. 4a). Typical diameter values were around a few tens of  $\text{k}\Omega \text{ cm}^2$ , however, with considerable scattering. This fact points to a different degree of passivation due to intermediate air contact and reactions in the aerated solution.

When the strongly acid anodisation solution at 40 °C is chosen also for EIS testing, the semicircle diameter

decreases by more than two orders of magnitude, but the shape of the total curve is not essentially altered (Fig. 4b). Obviously, a passive state still exists, although much less pronounced. Linear sweep voltammetric measurements confirmed that the situation at ocp is anodically controlled. The polarisation resistance amounted to  $0.11 \text{ k}\Omega \text{ cm}^2$ , which agrees principally with  $R_2$  as stated in Table 1.

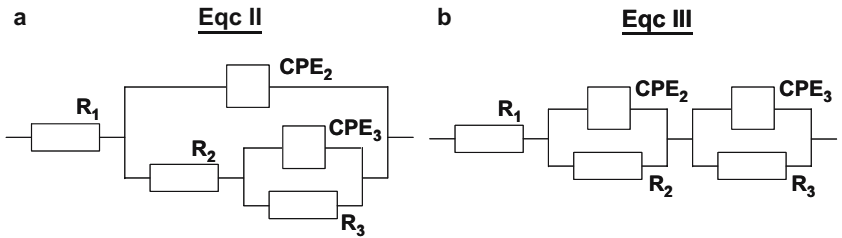
The behaviour with partially positive phase angles is similar to earlier findings on high purity Al in deaerated Na<sub>2</sub>CO<sub>3</sub> and H<sub>2</sub>SO<sub>4</sub>, respectively [22, 24]. This ‘inductive’ feature was ascribed to passivation or adsorption phenomena. For modelling, an  $R-C$  parallel combination with negative values was inserted into a Randles type network.

This approach was adapted here, leading to the inserted network Eqc I (Fig. 5), where  $R_2$  and CPE<sub>2</sub> are elements corresponding to the semicircle at high and intermediate  $f$ ,  $R_3$  and  $C_3$  are elements with negative signs corresponding to the loop, and  $R_4$  and  $C_4$  are elements corresponding to a second semicircle at very low  $f$ . Finally,  $R_1$  is connected with the outer electrolyte resistance between solid surface and Haber-Luggin capillary. The fitted parameters are summarised in Table 1 with the respective effective areas accounted for.

**Fig. 5** Equivalent circuit Eqc I

**Fig. 6** Bode plots for the anodised surface state P/SAAi in phosphate buffer at different exposure times (0.5 h—●, 18 h—□); for comparison, anodised state P/SAAu (18 h—◇) and pickled state P (—)

**Fig. 7** Equivalent circuits Eqc II and Eqc III



### Anodised surfaces

The impedance level (modulus  $|Z|$ ) owing to the state P/SAAi increased considerably in comparison with the pickled surface (Figs. 4 and 6). The extended exposure in PB up to 20 h did not show large changes in the EIS behaviour; however, a small decrease of  $|Z|$  in the range of the ‘plateau’ for  $f>50$  Hz was noticeable.

The situation with SAAu type systems is characterised by an extended nearly linear section in the  $\log|Z|-\log f$  plot (Fig. 6), which corresponds to the findings of Mansfeld and Kendig for SAAu-treated and sealed Al alloys in NaCl solution [19]. Compared with the SAAi spectrum, it is practically identical in the frequency range of lower than 10 Hz, whereas, the ‘plateau’ at medium frequency is more or less hidden.

Good fit results for the EIS spectra of the anodised systems were achieved using the model Eqc II (Fig. 7a), which is a simplified version of Eqc I. With capacitances instead of CPEs, it was principally introduced by Hoar and Wood for unsealed anodic SAAu films [18].

Here, the interleaved  $R_3||CPE_3$  elements would represent the impedance connected with the interface reactions and the solid state conduction in the barrier layer. On the other hand, the resistance  $R_2$  may be ascribed straightforward to the electrolyte resistance within the nano-sized pores of the porous sub-layer. Thus, this quantity reflects the (minor) changes during immersion due to restructuring reactions in the gel-like porous layer substances. On the other hand, EIS reveals noticeable differences in the porous sub-layers of the SAAi and the SAAu type under the test conditions. The slight differences of the nano-pore diameters is one of the reasons for this finding. The precise effect of the

considerable micro-roughness in the SAAi case is unfortunately unclear.

The fitted data are summarised in Table 2.

It should be noted that even better fitting results could be achieved with a model essentially consisting of two serial  $R||CPE$  combinations (Eqc III, Fig. 7b). Such a network with simple capacitances, instead of CPEs, was used by Paatsch and Lorenz [20] for anodised and sealed materials. The two separate  $R-C$  pairs were associated with both sub-layers, which are, strictly considered, not two separate entities. Corresponding to the altered combination of circuit elements, the individual fit values reach different values (Table 3).

In the case of the P/SAAu layers, the parameters of the characteristic pair  $R_2||CPE_2$  amount to  $2.1 \text{ M}\Omega \text{ cm}^2$  and  $2.5 \mu\text{F cm}^{-2}$  (0.97) ( $\chi^2=0.0078$ ) for the instantaneous measurement. With prolonged exposure, the following values were determined for  $R_2||CPE_2$ :  $0.19 \text{ M}\Omega \text{ cm}^2$  and  $68 \mu\text{F cm}^{-2}$  (0.60) ( $\chi^2=0.0032$ ). Based on the serial modelling of Eqc III, the differences in the pore-related properties of the two layer types considered appear to be much more pronounced than using Eqc II.

The EIS response of additional sealing measures is documented elsewhere [23].

### Chemically modified surfaces (P/SAAi/C)

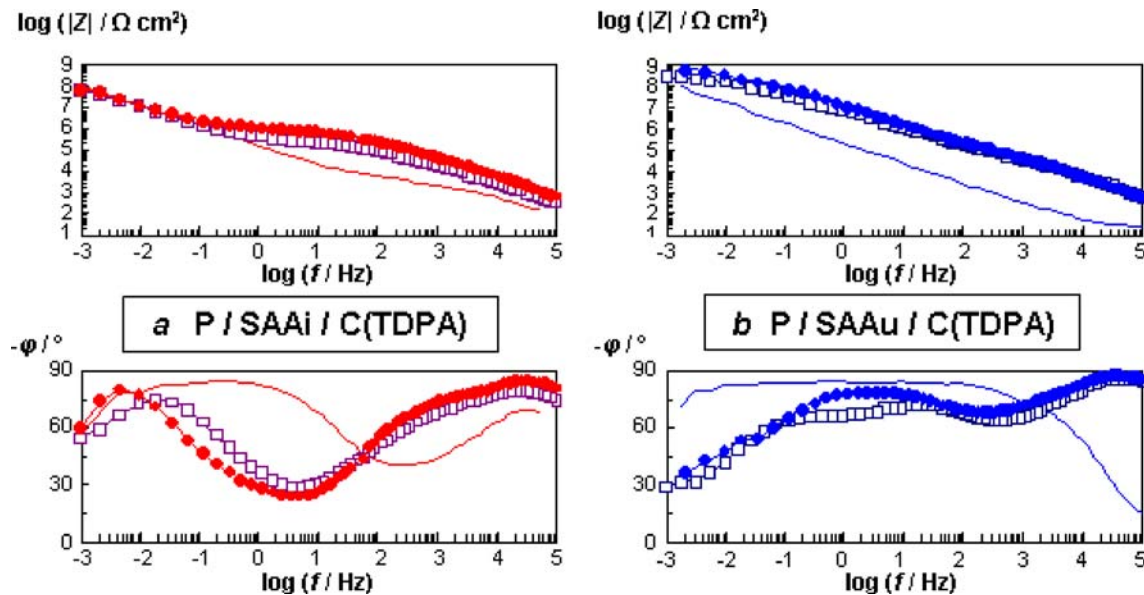
The treatment of SAAi specimens with solutions of different hydrophobising substances and subsequent exposure to aqueous solutions provided evidence that the EIS behaviour altered, but not in the same way.

**Table 2** Numerical values based on model Eqc II for the surface types P/SAAi and P/SAAu in phosphate buffer after different exposure time

|                | $R_1/\Omega \text{ cm}^2$ | $R_2/\text{k}\Omega \text{ cm}^2$ | $CPE_2/\mu\text{F cm}^{-2}$ | $R_3/\text{M}\Omega \text{ cm}^2$ | $CPE_3/\mu\text{F cm}^{-2}$ | $\chi^2$ |
|----------------|---------------------------|-----------------------------------|-----------------------------|-----------------------------------|-----------------------------|----------|
| P/SAAi; >0.5 h | 12                        | 5.4                               | 0.27 (0.80)                 | 337                               | 0.76 (0.94)                 | 0.021    |
| P/SAAi; >18 h  | 39                        | 3.0                               | 0.29 (0.83)                 | 572                               | 0.70 (0.94)                 | 0.027    |
| P/SAAu; >0.5 h | 24                        | 1.8                               | 0.44 (1.0)                  | 57 (?)                            | 0.43 (0.82)                 | 0.0040   |
| P/SAAu; >18 h  | 27                        | 0.63                              | 0.54 (0.96)                 | 495                               | 0.26 (0.95)                 | 0.023    |

**Table 3** Numerical values based on model Eqc III for the surface type P/SAAi in phosphate buffer after different exposure time

|                          | $R_1/\Omega \text{ cm}^2$ | $R_2/\text{k}\Omega \text{ cm}^2$ | $CPE_2/\mu\text{F cm}^{-2}$ | $R_3/\text{M}\Omega \text{ cm}^2$ | $CPE_3/\mu\text{F cm}^{-2}$ | $\chi^2$ |
|--------------------------|---------------------------|-----------------------------------|-----------------------------|-----------------------------------|-----------------------------|----------|
| Phosphate buffer, >0.5 h | 6E-7                      | 3.4                               | 1.9 (0.66)                  | 345                               | 1.0 (0.94)                  | 0.0049   |
| Phosphate buffer, >18 h  | 4E-5                      | 3.1                               | 1.5 (0.69)                  | 355                               | 1.0 (0.93)                  | 0.0055   |



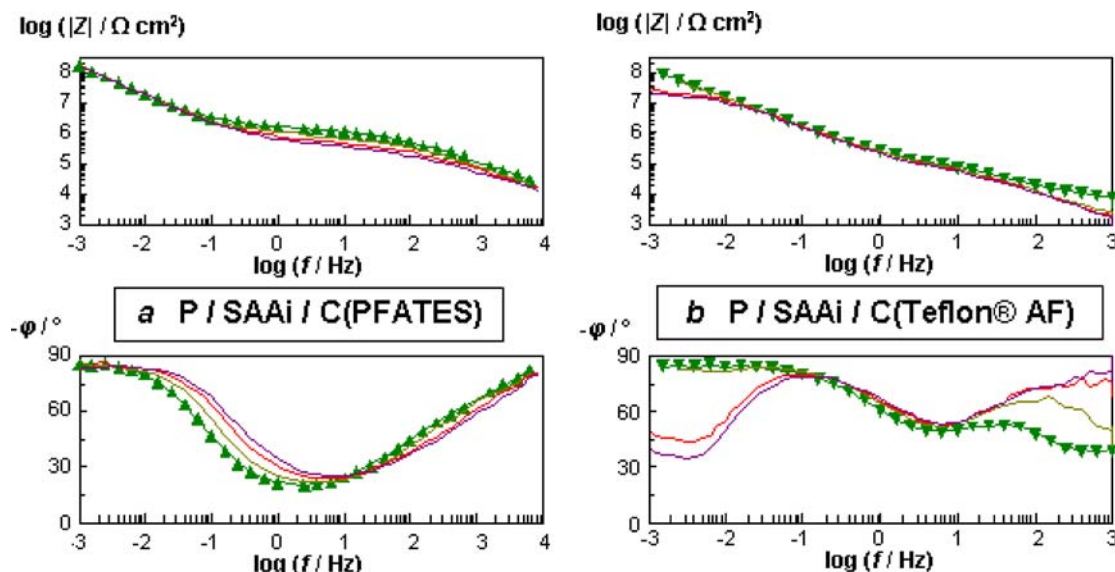
**Fig. 8** Bode plots for the surface states P/SAAi/C(TDPA) (**a**) and P/SAAu/C(TDPA) (**b**) in phosphate buffer at different exposure times (0.5 h ●, 18 h □); states P/SAAi and P/SAAu (—) for comparison

Figure 8 displays the situation after the treatment with *tetradecanephosphonic acid* (TDPA), which will form self-assembled monolayers. The impedance behaviour of the P/SAAi/C surface shows a similar shape to the corresponding initial state P/SAAi; however, the  $|Z|$  plateau shifted to considerably higher values and lower frequencies (Fig. 8a). As such a shape is related to porosity phenomena with paint layers [19, 20], it appears reasonable to conclude that the oxide-related nano-porosity only has been modified by the penetrating organic agent, but is still existent. This is a principal difference to systems which were given a thick and vastly pore-free coating, e.g. by painting. In the low-frequency region, even a coincidence of the spectra is

observed. This region is determined by the properties of the barrier layer.

In contrast, with P/SAAu/C, a general impedance increase was measured (Fig. 8b) with only minor changes in the  $\log|Z|$ - $\log f$  curve shape. Moreover, the changes due to prolonged exposure seem less pronounced than in the case P/SAAi/C(TDPA).

Modelling was accomplished based on an equivalent circuit with three or four serial  $R||CPE$  elements. Such an arrangement may appear to be not very reasonable from a physical point of view, which should be an essential criterion of modelling approaches. Rather, it accounts for the observed inclined, ‘smeared’ log-log course, which



**Fig. 9** Bode plots for the surface states P/SAAi/C(PFATES) (**a**) and P/SAAi/C(Teflon AF) (**b**) in  $\text{Na}_2\text{SO}_4$  at different exposure times (start 0.1 h-triangles, 2 h, 6 h, 10 h-lines)

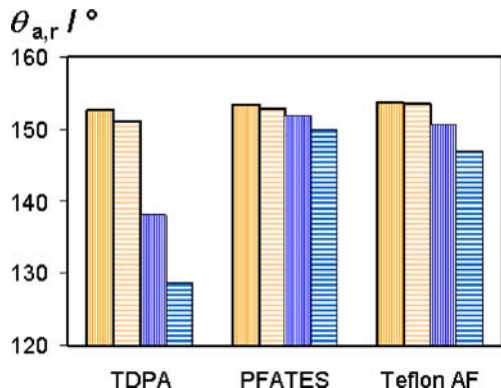


**Fig. 10** Comparison of the wetting data ( $\theta_a$ —vertically striped pattern,  $\theta_r$ —horizontally striped pattern) for differently coated specimen types in their original states (orange, bold faced lines) and after the simulating weathering test according to DIN EN ISO 11341 (blue)

may be a result of lateral surface inhomogeneity. On this basis, good fit results were achieved, as the  $\chi^2$  values demonstrate 0.063 and 0.0039 for the measurements of Fig. 8a; 0.0033 and 0.013 for those of Fig. 8b.

Figure 9 shows EIS results obtained for two representative specimens with alternative modification, namely, using the *reactive fluoroalkylsilane PFATES* and the *fluorocopolymerTeflon® AF* (following the intermediate treatment with the aminosilane AEAPS), respectively. The  $\log|Z|-\log f$  curves for the PFATES-modified surface display a constant shape with a plateau at medium frequencies (Fig. 9a), which points again to still existing nano-porosity in the modified oxidic layer. The impedance level decreases monotonically with increasing exposure time. Thus, this situation is nearly identical with that for TDPA-modified specimens (Fig. 8a).

However, in the case of the AEAPS-/ copolymer-modified surface, another EIS behaviour occurs. The shape of the curves deviates from the former ones, and prolonged exposure leads to changes in different frequency ranges (Fig. 9b). Thus, immersion causes different chemical and/or physical changes in the layer system.

An exposure-related *increase* of the total impedance was observed in neither of the examined systems in contrast to the measurements with bis-silan-treated Al alloy after incomplete curing [29]. The different pattern of impedance change is due to the considerably deviating water content of the treating solution, which had led to a certain degree of (primary) hydrolysis, to a much higher film thickness (350 nm) with a high amount of reactive groups in the film substance and, finally, to condensation and cross-linking reactions during the immersion in the aqueous test medium.

Interestingly, the observed EIS behaviour does not directly correlate with the real degradation process, which consists of desorption or hydrolytic reactions resulting in turn in the displacement of the hydrophobising substances (by water under participation of ions) and the loss of the water repellency. The experiments showed that the TDPA-modified specimens were, as a rule, completely hydrophilic

after the 20-h exposure in the phosphate-buffered solution, whereas, the PFATES-treated surfaces revealed no deterioration at all, although there was a quite similar EIS behaviour. The Teflon® AF-modified specimens showed a slight decrease in water repellency.

These observations are confirmed by the results of standardised weathering tests (DIN EN ISO 11341). The degradation of the wetting data after passing this test can be seen from Fig. 10. From the degree of the measured changes, an ascending ranking order of the stability upon dewing/drying and light radiation can be derived: TDPA << AAPS/Teflon® AF < PFATES.

Obviously, EIS evaluates among other parameters the resistive properties of the nano-pores, whereas, the wetting behaviour depends preferentially on the morphologic and chemical properties of the *utmost* surface. A reasonable prediction of the wetting behaviour and its stability from EIS will, therefore, be critical.

## Conclusions

Ultrahydrophobic surfaces of aluminium materials were successfully generated based on an acid anodisation process under intensified temperature and current density conditions (SAAi) and a subsequent chemical modification step (thin-film coating). Electrochemical impedance spectrometry (EIS) was used to characterise the individual material states including ultrahydrophobic surfaces and to derive appropriate equivalent circuit models.

The impedance spectra gained information on characteristic features and parameters. With mostly very good fit results, some refinement should be done in the cases of less descriptive equivalent circuits.

For the specimen types treated with alkylphosphonic acid or fluoroalkylsilane, the measurements allowed the conclusion that the nano-porosity of the SAAi-formed oxidic layers underwent marked changes due to the chemical modification, but the pores remained principally accessible. With copolymer-modified surfaces, a different situation occurs.

The characterisation is amended at present by *in situ* measurements of the coating kinetics using of a quartz crystal micro-balance.

The prediction of the water repellency and weathering stability proved to be difficult for EIS, as the impedance was mainly influenced by the interior of the oxidic layer, whereas, the wetting properties during the respective exposure are determined by the *utmost* surface with its morphological and chemical features.

**Acknowledgements** The authors are indebted to U Cikalo, R Süptitz (Technische Universität Dresden), S Schmidt and R Frenzel (Leibniz Institut für Polymerforschung Dresden) for valuable experimental contributions and discussion. The financial support by the Sächsisches Staatsministerium für Wissenschaft und Kunst (contract no. 4-7533-70-821-98/3) and the Bundesministerium für Bildung und Forschung (FKZ 03C0340B) is gratefully acknowledged.

---

## References

1. Dettner HW, Elze J (1974) Handbuch der Galvanotechnik. Hanser, München
2. Jelinek TW (1997) Oberflächenbehandlung von Aluminium. Leuze, Saulgau
3. Shvabe K, Zushke KhD, Time M (1974) *Zasc Met* 10:491
4. Schwabe K, Quy N (1963) *Mber Dtsch Akad Wiss Berl* 5:372
5. Nielsch K, Choi J, Schwirn K, Wehrspohn RB, Gösele U (2002) *Nanoletters* 2:677
6. Strawbridge A, Gabe DR, Dowell AJ (1990) *Trans Inst Met Finish* 68:69
7. Tsujii K, Yamamoto T, Onda T, Shibuichi S (1997) *Angew Chem* 109:1042; Shibuichi S, Yamamoto T, Onda T, Tsujii K (1998) *J Colloid Interface Sci* 208:287
8. Thieme M, Frenzel R, Schmidt S, Simon F, Hennig A, Worch H, Lunkwitz K, Scharnweber D (2001) *Adv Eng Mater* 3:691
9. Thieme M, Frenzel R, Hein V, Worch H (2003) *J Corros Sci Eng* 6: paper 47
10. Barthlott W, Neinhuis C (1997) *Planta* 202:1
11. Neinhuis C, Barthlott W (1997) *Ann Bot* 79:667
12. Blossey R (2003) *Nat Mater* 2:301
13. Reihs K et al (2000) WO 00/39240
14. Marmur A (2003) *Langmuir* 19:8343
15. McHale G, Shirtcliffe NJ, Newton MI (2004) *Langmuir* 20:10146
16. Blank C, Frenzel R, Hein V, Schmidt B, Simon F, Thieme M, Tittes K, Worch H (2004) In: Pohl M (ed) *Fortschritte der Metallographie, Sonderband 36 der Prakt. Metallographie, Werkstoff-Informationsgesellschaft*, Frankfurt, p 491
17. Schwabe K, Schmidt W (1970) *Corros Sci* 10:143
18. Hoar TP, Wood GC (1962) *Electrochim Acta* 7:333
19. Mansfeld F, Kendig M (1984) In: *Proceedings of the 9th international conference on metallic corrosion*, Toronto, p 74
20. Paatsch W, Lorenz WJ (1986) In: Heitz E, Rowlands JC, Mansfeld F (eds) *Proceedings of International Workshop, Ferrara 1985*, Dechema, Frankfurt, p 221
21. Thieme M, Linck J (1988) *Werkstoffe und Korrosion* 39:465
22. Moon SM, Pyun SI (1998) *J Solid State Electrochem* 2:156
23. Tittes K, Schmidt B, Blank C, Hein V, Worch H, Simon F, Frenzel R (2004) In: *GdCh-Monographie Bd. 32*, Frankfurt, p 176
24. Fernandes JCS, Ferreira MGS, Rangel CM (1990) *J Appl Electrochem* 20:874
25. Pajkossy T, Nyikos L (1986) *J Electrochem Soc* 133:2061; Pajkossy T, Nyikos L (1989) *Electrochim Acta* 34:181 and earlier publications
26. Rammelt U, Reinhardt G (1990) *Electrochim Acta* 35:1045
27. Rammelt U, Schiller CA (2000) *Models in Chem* 137:199
28. Lange R et al. (2002) 17th Conference ESB, Barcelona, p 90
29. Van Ooij WJ, Zhu D (2001) *Corrosion* 57:413; Zju D, van Ooij WJ (2001) The third international symposium on silanes and other coupling agents, Newark, New Jersey, June 18–19
30. Harm U, Fürbeth W, Mangold KM, Jüttner K (2002) *Macromol Symp* 187:65
31. Frankel GS (2003) *J Corros Sci Eng* 6: paper 16
32. Liakos IL, Newman RC, McAlpine E, Alexander MR (2004) *Surf Interface Anal* 36:347
33. Jander G (1989) *Massanalyse*. De Gruyter, Berlin, New York